

This document is confidential and is proprietary to the American Chemical Society and its authors. Do not copy or disclose without written permission. If you have received this item in error, notify the sender and delete all copies.

Mass Transfer through Vapor-Liquid Interfaces studied by Non-Stationary Molecular Dynamics Simulations

Journal:	<i>The Journal of Physical Chemistry</i>
Manuscript ID	jp-2022-08752y
Manuscript Type:	Article
Date Submitted by the Author:	14-Dec-2022
Complete List of Authors:	Schaefer, Dominik; TU Kaiserslautern, Laboratory of Engineering Thermodynamics (LTD) Stephan, Simon; Technische Universität Kaiserslautern Fachbereich Maschinenbau und Verfahrenstechnik, Laboratory of Engineering Thermodynamics Langenbach, Kai; Universität Innsbruck, Institut für Chemieingenieurwissenschaften Horsch, Martin; Norwegian University of Life Sciences, Faculty of Science and Technology, Department of Data Science Hasse, Hans; Technische Universität Kaiserslautern, Laboratory of Engineering Thermodynamics (LTD)

SCHOLARONE™
Manuscripts

1
2
3 **Mass Transfer through Vapor-Liquid Interfaces studied by Non-Stationary Molecular**
4 **Dynamics Simulations**
5

6
7 Dominik Schaefer,¹ Simon Stephan,^{1, a)} Kai Langenbach,² Martin T. Horsch,³ and Hans
8 Hasse¹
9

10 ¹⁾*Laboratory of Engineering Thermodynamics (LTD), TU Kaiserslautern,*
11 *67663 Kaiserslautern, Germany*
12

13 ²⁾*Institute of Chemical Engineering, University of Innsbruck, 6020 Innsbruck,*
14 *Austria*
15

16 ³⁾*Norwegian University of Life Sciences, Faculty of Science and Technology,*
17 *Department of Data Science, Drøbakveien 31, 1430 Ås,*
18 *Norway*
19

20 (Dated: Wed 14th Dec, 2022)
21
22
23
24
25
26
27
28
29
30
31
32
33
34
35
36
37
38
39
40
41
42
43
44
45
46
47
48
49
50
51
52
53
54
55
56
57
58
59
60

Abstract:

Molecular dynamics (MD) simulations are highly attractive for studying the influence of interfacial effects, such as the enrichment of components, on the mass transfer through the interface. In a recent work, we have presented a steady-state MD simulation method for investigating this phenomenon and have tested it using model mixtures with and without interfacial enrichment. The present study extends this work by introducing a non-stationary MD simulation method. A rectangular simulation box that contains a mixture of two components 1 + 2 with a vapor phase in the middle and two liquid phases on both sides is used. Starting from a vapor-liquid equilibrium state, a non-stationary molar flux of component 2 is induced by inserting particles of component 2 into the center of the vapor phase in a pulse-like manner. During the isothermal relaxation process, particles of component 2 pass through the vapor phase, cross the vapor-liquid interface, and enter the liquid phase. The system thereby relaxes into a new vapor-liquid equilibrium state. During the relaxation process, spatially resolved responses for the component densities, the fluxes, and the pressure are sampled. To reduce the noise and provide measures for the uncertainty of the observables, a set of replicas of simulations is carried out. The new simulation method was applied to study mass transfer in two binary Lennard-Jones mixtures: one that exhibits a strong enrichment of the low-boiling component 2 at the vapor-liquid interface and one that shows no enrichment. Even though both mixtures have similar transport coefficients in the bulk phases, the results for the mass transfer differ significantly, indicating that the interfacial enrichment influences the mass transfer.

Keywords: vapor-liquid interface, mass transfer, binary mixture, Lennard-Jones fluid, molecular dynamics, simulation method, non-stationary, enrichment

^{a)}Electronic mail: simon.stephan@mv.uni-kl.de

I. INTRODUCTION

Mass transfer through vapor-liquid interfaces is a highly important phenomenon: it is ubiquitous in nature and applied in many technical processes, including fluid separation processes, such as absorption and distillation. While macroscopic mass transfer theories generally consider the interface as a two-dimensional object, it is well known from molecular studies that an interfacial region exists, in which the intensive properties change from the value in one bulk phase to that in the other in a continuous manner, involving steep gradients, as the interfacial region is only a few nanometers wide. Interesting phenomena occur in the interfacial region, such as the enrichment of components¹⁻¹⁴. The vapor-liquid interfacial region has been studied extensively in equilibrated systems, but only little is known on the influence of mass transfer on that region and, vice versa, on the influence of that region on mass transfer. That influence is usually neglected in macroscopic mass transfer theories, but, recently, doubts on the validity of that assumption have been raised^{7,10,15-21}, which makes such studies all the more important.

Molecular dynamics (MD) simulations are ideally suited for investigating mass transfer through interfaces on the molecular level. Given the importance of this phenomenon, it is astonishing that, up to recently, no MD simulation methods for studying mass transfer through vapor-liquid interfaces driven by a gradient in the chemical potential have been described in the literature. We have, therefore, devised and tested two such methods. The first one is based on stationary simulation and has been published recently²². The second one, a non-stationary method, is described in the present work and tested using the same mixtures as in the tests of the first method. In these simulations, we address the question whether an interfacial enrichment has an influence on the mass transfer rates. The approach we take for this is straightforward: we compare results for fluxes through interfaces in a model mixture with a high interfacial enrichment with those obtained for a similar mixture that has no enrichment.

Heat transfer through vapor-liquid interfaces during evaporation and condensation has been frequently investigated in the literature using molecular simulations²³⁻⁴² and continuum models such as *density functional theory* (DFT)^{31,36,40,42-46}. This inherently involves mass transfer, but the focus of the studies is different from ours; furthermore, in most of these studies, only pure components were considered. Stationary mass transfer through pores,

1
2
3 membranes, crystals^{47–53}, and homogeneous fluid phases^{54–56} induced by a gradient of the
4 chemical potential has been subject of several studies. However, these studies do not involve
5 vapor-liquid interfaces. In these studies, the gradient was usually created using the so-called
6 dual-control volume (DCV) method^{49,52,57–59}. In the recent work of our group²², that was
7 already mentioned above, we have adapted the DCV method to induce a stationary flux of a
8 component through the vapor-liquid interface of a binary mixture. The simulation method
9 for quasi-stationary mass transfer through a vapor-liquid interface driven by a gradient in the
10 chemical potential was adapted in a recent study by *Rauscher et al.*⁶⁰ with the extension of a
11 temperature gradient to investigate mass and heat transfer at interfaces of similar mixtures
12 of simple fluids.

13
14
15
16
17
18
19
20
21 Non-stationary mass transfer close to and in the interfacial region has been investigated by
22 several studies using different techniques: *Baidakov et al.*^{61,62} have investigated the dynamic
23 formation of vapor-liquid interfaces in pure substances and binary mixtures and the evolution
24 of interfacial properties in the process. In their studies, first a system containing a coexisting
25 vapor and liquid phase was equilibrated. After the equilibration, all particles in the interface
26 layer were instantaneously removed and the non-stationary relaxation process and formation
27 of a new vapor-liquid interface was observed. *Bucior et al.*⁶³ have studied evaporation of a
28 pure liquid in a slit pore into a spontaneously created vacuum by moving the pore walls. *Nagl*
29 *et al.*¹⁵ studied the non-stationary mass transfer through liquid-liquid interfaces of different
30 real fluid mixtures using a combination of experiments and theoretical calculations. *Braga*
31 *et al.* investigated self-diffusion at liquid-liquid interfaces⁶⁴ and the free energy barrier at
32 vapor-liquid interfaces⁶⁵ by moving a probe particle through the respective interface. *Garrett*
33 *et al.*⁶⁶ observed the trajectories of single particles moving in the vicinity of a vapor-liquid
34 interface in aqueous systems under equilibrium conditions and categorized four different
35 behaviors of these particle: adsorption, absorption, desorption, and reflection.

36
37
38
39
40
41
42
43
44
45
46
47 In the present work, we describe a new simulation method for studying a non-stationary
48 mass transfer through vapor-liquid interfaces of mixtures: First, the system containing only
49 particles of one component is equilibrated. The initial equilibrium state consists of a liquid
50 phase slab surrounded by a vapor bulk phase, which coexist in a rectangular simulation
51 box with periodic boundary conditions. After the first equilibration, particles of a second
52 component are inserted in the middle of the vapor phase during a short period of time, i.e. in
53 a pulse-like manner. This perturbation induces a non-stationary, one dimensional flux of the
54
55
56
57
58
59
60

1
2
3 inserted particles towards the two vapor-liquid interfaces and through them into the liquid
4 phase on both sides of the vapor phase. The process is basically symmetric with regard to
5 these interfaces. The relaxation process caused by the perturbation is then studied, focusing
6 on the processes in the vicinity of the interfaces. Simulations are run until a second, final
7 equilibrium state is reached.
8
9

10
11 A major problem of non-stationary molecular dynamics simulations is to distinguish
12 an actual physical process from random noise and to provide a measure of uncertainty.
13 Therefore, our simulation study was performed using *sets of replicas*, i.e. the simulation was
14 repeated several times using different initial velocity distributions. The simulation box and
15 start system size, temperature, and the insertion procedure were the same for all simulations
16 in a set of replicas. The results obtained from a set of replicas were averaged, resulting in a
17 reduction of the noise of the signal; furthermore, a measure for the statistical uncertainties
18 of the observables was obtained. This replica strategy based on varying starting conditions
19 is a well-established method in non-stationary molecular dynamics simulations^{65,67-70}.
20
21
22
23
24
25
26
27

28 The new simulation method was applied to investigate non-stationary mass transfer in two
29 binary Lennard-Jones mixtures with distinctively different phase behavior. Both mixtures
30 (referred to as mixture A and B in the following) have been studied extensively by our
31 group regarding thermodynamic^{10,16,71-73} and transport properties²². Equilibrium molecular
32 dynamics simulations and density gradient theory consistently yield a strong enrichment of
33 the low-boiling component at the interface for mixture A, while no such enrichment is found
34 in mixture B^{10,16,22,71-73}. The same mixtures have been used in the quasi-stationary approach
35 of our recent study²².
36
37
38
39
40
41

42 An enrichment of low-boiling components at equilibrium conditions has been reported
43 for many mixtures of real fluids and model fluids¹⁻¹³; see Ref.⁷⁴ for a recent review. It has
44 been discussed in various studies^{7,10,15-21} that the enrichment might have an influence on the
45 diffusive mass transfer through the interface (which would be in line with Fick's law), but
46 to date there is no proof of this hypothesis. No experimental studies of this are available,
47 nor are they to be expected in the foreseeable future, since the enrichment occurs in the
48 interfacial region, which is only a few nanometers wide and fluctuates, which hinders the
49 acquisition of meaningful experimental data. Hence, we have to rely on simulation methods
50 for corresponding studies.
51
52
53
54
55
56

57 This paper is structured as follows: First, the simulation method is introduced. Then, the
58
59
60

1
2
3 studied test mixtures are described. Next, the simulation results from one temperature are
4 discussed in detail comparing the results from both mixtures. Finally, results obtained for
5 several temperatures are compared, which provides insights into the temperature dependency
6 of the relaxation process.
7
8
9

10 11 12 **II. SIMULATION METHOD**

13 14 15 **A. Overview**

16
17
18 The basic concept of the simulation method is illustrated in Figure 1. The simulation box
19 has a rectangular shape and periodic boundary conditions in all directions. At the start, the
20 simulation box only contains particles of component 1. The conditions are chosen so that
21 the box contains two phases: a vapor phase in the middle of the simulation box surrounded
22 by a liquid phase. During the entire simulation run, the number of particles of component 1,
23 the temperature, and the volume of the simulation box are kept constant. After establishing
24 the vapor-liquid equilibrium state of the pure component 1 system, it is perturbed by the
25 insertion of particles of component 2, which are inserted in the control volume (CV) in the
26 middle of the vapor phase, cf. Figure 1. The response of the system to that perturbation is
27 evaluated until the system relaxes into a second vapor-liquid equilibrium state. Except for
28 statistical fluctuations, the process is symmetric with respect to a plane in the middle of the
29 simulation box.
30
31
32
33
34
35
36
37

38
39 Hence, a simulation run consists of the following five phases:

- 40
41 1. Initial equilibration phase (*IniEq*)
- 42
43 2. Sampling phase of the first vapor-liquid equilibrium state (*Eq1*)
- 44
45 3. Insertion phase (*In*)
- 46
47 4. Relaxation phase (*Relax*)
- 48
49 5. Sampling phase of the second vapor-liquid equilibrium state (*Eq2*)
50
51
52
53

54 The abbreviations in the brackets are used in the following for brevity.

55
56 The first two simulation phases *IniEq* and *Eq1* are carried out in the *NVT* ensemble.
57 Subsequently, in the *In* phase, particles of component 2 are inserted in the center of the
58
59
60

vapor bulk domain, cf. Figure 1. The insertion of particles of component 2 inside the control volume is performed using a Monte Carlo algorithm^{54,57,58}, that adjusts the number of particles of the component 2 based on a prescribed chemical potential of that component $\mu_{2,CV}$. Since the chemical potential is only controlled in a sub-volume of the entire simulation box (cf. Figure 1), the *In* phase can be considered a quasi- μVT ensemble.

With the beginning of the particle insertion, a one dimensional, non-stationary molar flux j_2 of particles of component 2 is established. The molar flux is positive on the right of the control volume and negative on the left of the control volume due to the symmetry of the simulation box setup, cf. Figure 1. During the *Relax* phase the system re-equilibrates to the second equilibrium state point, which is sampled over the course of the *Eq2* phase. The *Relax* and the *Eq2* phase are again carried out in the *NVT* ensemble.

B. Definition of Observables and Data Processing

The simulation box is discretized in z -direction into 1,200 equally sized bins. Since a planar interface is studied, no bin-discretization in x - and y -direction is applied, i.e. the simulation scenario is quasi-one-dimensional. Observables $\chi(\tau, z)$ are sampled in these bins as a function of the z -direction and time τ every 10,000 simulation steps. The studied observables are the pressure tensor p , the density ρ_i , and the mole composition x_i of a component i . The rate of change of the density $\partial\rho_i/\partial\tau(\tau, z)$, which is needed for the determination of the molar flux j_i , is determined for each bin separately by numerical differentiation with respect to the time τ .

The position of the liquid film and its interfaces is not fixed in the simulation box and can therefore freely move during the simulation run (it fluctuates and changes slightly due to the absorption of component 2). The positions $z_{50} = z(\rho_{50})$ of the two interfaces as well as the positions $z_{10} = z(\rho_{10})$ and $z_{90} = z(\rho_{90})$ were determined by the z -position, where the local total density corresponds to 10 %, 50 %, and 90 % of the bulk density difference, i.e.

$$\begin{aligned}\rho_{10} &= \rho'' + 0.1(\rho' - \rho'') , \\ \rho_{50} &= \rho'' + 0.5(\rho' - \rho'') , \\ \rho_{90} &= \rho'' + 0.9(\rho' - \rho'') ,\end{aligned}\tag{1}$$

where ρ'' indicates the total vapor bulk phase density and ρ' the total liquid bulk phase

density. Details on the procedure to determine ρ'' and ρ' are given in the Supporting Information.

In the following, the data processing procedure is described for the right interface only (cf. Figure 1). The interface on the left is evaluated applying an equivalent procedure and results for both interfaces are averaged. The molar flux j_2 of the inserted particles of component 2 is determined by solving the molar balance of each bin per time step. Particles of component 2 may enter or leave a bin over its two boundaries, thus there are two molar flux j_2 per bin. The molar flux j_2 is always the net molar flux here. A positive flux is directed in positive z -direction and, accordingly, a negative flux is directed in negative z -direction. In the following, the index $n = 1 \dots N$ denotes bins and the flux at the left bin boundary has the index n while the flux at the right bin boundary has the index $n+1$. The molar balance of a bin n for particles of component 2 at a time step τ can therefore be written as

$$\frac{\partial \rho_2}{\partial \tau}(\tau, n) = -\frac{j_2(\tau, n+1) - j_2(\tau, n)}{\Delta z_{\text{bin}}}, \quad (2)$$

where Δz_{bin} is the size of the bin and j_2 is the molar flux of component 2. To obtain $N+1$ unknown molar fluxes of N bins, N molar balances have to be solved (cf. Eq. (2)) with the help of a boundary condition. In this work, the symmetry boundary condition applies, according to which the net flux in the middle of the liquid slab is zero (cf. Figure 1). The position of the middle of the liquid slab is determined as the midpoint between the positions z_{50} of the two interfaces in each time-step and, hence, may fluctuate during the simulation. The gradient and molar balances are determined in a fixed reference frame in each time step, only the position, where the symmetry boundary condition is applied, moves according to the position of the middle of the liquid slab. This is done for each simulation in a set of replicas independently and results are averaged at the position of the middle of the liquid slab. The density, composition, and pressure tensor sampled in a bin n at the same time τ are averaged over all simulations in a set of replicas. This procedure significantly reduces noise and enables the estimation of the statistical uncertainty for each sampled observable χ .

The start and end time of the In phase are the same for all simulations. The number of inserted particles in a set of replicas varies due to the probabilistic nature of the Monte Carlo algorithm. The number for $\mu_{2,\text{CV}}$ was chosen so that the mean number of inserted particles in set of replicas was 1,200 particles. The distribution of the number of inserted particles in a set of replicas is quite narrow (standard deviation about 1.5 %). Preliminary

tests showed that this yields a satisfactory signal-to-noise ratio for the observables of interest such as density, pressure, and molar flux during the simulation run. Details are given in the Supporting Information.

The behavior of the system in the vapor phase and the liquid phase in the vicinity of the vapor-liquid interface is of particular interest. The relaxation process is sampled in two measurement volumes (MV) close to the interface: one in the bulk vapor phase and one in the bulk liquid phase (here labeled with MV_{vap} and MV_{liq} , respectively). The position of these measurement volumes is defined with respect to the interface position, as illustrated in Figure 2. Figure 3 illustrates the simulation procedure, the responses to the perturbation in vapor and liquid phase determined from a set of replicas as well as the five phases of the non-stationary simulation method.

III. APPLICATION OF THE SIMULATION METHOD

A. Binary Lennard-Jones Mixtures

The Lennard-Jones (LJ) fluid is computationally inexpensive, but is able to reliably describe properties of simple fluids^{75,76}, which makes it well-suited for testing new methods in molecular simulations. In the present work, the so-called truncated and shifted Lennard-Jones potential (LJTS) was used, with a cut off radius of $r_c = 2.5 \sigma$:

$$u_{\text{LJ}}(r) = 4\epsilon \left[\left(\frac{\sigma}{r} \right)^{12} - \left(\frac{\sigma}{r} \right)^6 \right] \quad \text{and} \quad (3)$$

$$u_{\text{LJTS}}(r) = \begin{cases} u_{\text{LJ}}(r) - u_{\text{LJ}}(r_c) & r \leq 2.5 \sigma \\ 0 & r > 2.5 \sigma \end{cases} \quad (4)$$

Here, $u_{\text{LJ}}(r)$ is the potential energy of the LJ potential between the particles⁷⁷, which depends on their distance r . For the cross-interactions of unlike particles in the mixtures, the modified Lorentz-Berthelot combination rules were applied^{78,79}

$$\sigma_{ij} = \frac{\sigma_i + \sigma_j}{2} \quad (5)$$

$$\epsilon_{ij} = \xi_{ij} \sqrt{\epsilon_i \epsilon_j} \quad (6)$$

in which an additional binary parameter ξ_{ij} is introduced (cf. Eq. (6)), which has an important influence on the phase behavior of binary mixtures⁷¹.

The simulation method proposed in this work is applied to two different binary LJTS mixtures. For both mixtures, the size parameter σ_i and mass m_i of component 1 and 2 are equal and set to unity. Also the energy parameter of component 1 ε_1 is set to unity while ε_2 of the components 2 is different for the two mixtures. The same holds for ξ_{12} . The parameters of the two studied test mixtures are given as:

- Mixture A: $\varepsilon_2/\varepsilon_1 = 0.6$ and $\xi_{12} = 0.85$
- Mixture B: $\varepsilon_2/\varepsilon_1 = 0.9$ and $\xi_{12} = 1.00$

The phase behavior and interfacial properties of these two LJTS mixtures have been investigated systematically in previous works of our group^{10,16,71–73}. Their thermophysical properties were therein found to be well described by the PeTS equation of state^{10,80}. The resulting phase equilibria of the mixtures A and B at the temperatures that were studied in the present work are shown in Figure 4. Mixture A has an asymmetric, wide-boiling phase behavior, whereas mixture B has essential an ideal phase behavior in the sense of Raoult’s law. Mixture A also exhibits a vapor-liquid-liquid equilibrium (VLLE) at the lowest studied temperature. Even though both mixtures have distinctively different phase behaviors, they have similar diffusivity (the product of density and the mutual diffusion coefficient) in the vapor and liquid phases²². In mixture A, the low-boiling component exhibits a large enrichment at the vapor-liquid interface in thermodynamic equilibrium^{10,72}, i.e. the number density $\rho_2(z)$ shows a distinct maximum at the interface. In mixture B, no such enrichment is present.^{10,72} The two mixtures also differ in other interfacial properties such as the surface tension, the interfacial thickness, and the relative adsorption of the low-boiling component at the interface; for details see⁷².

In the following, all physical properties are reduced using the LJ potential parameters of the high-boiling component 1 ($\sigma_1, \varepsilon_1, m_1$) (which are equal for both considered mixtures) and the Boltzmann constant k_B ^{77,81}.

B. Simulation Details

For the simulations carried out in this work, the simulation box had a rectangular shape with a length l_z in z -direction of $l_z = 150\sigma$ and a quadratic cross section in x - and y -direction with a side length of $l_y = l_x = 27.85\sigma$. The temperature was controlled by the

1
2
3 velocity scaling thermostat⁷⁷. The control volume had a length in z -direction of $\Delta z_{CV} = 10 \sigma$
4 and the same quadratic cross section in x - and y -direction as the simulation box. The
5 time step was $\Delta \tau = 0.001 \sigma(m/\varepsilon)^{1/2}$. The total run time was $\Delta \tau_{\text{Sim}} = 4,500 \sigma(m/\varepsilon)^{1/2}$ for all
6 simulations. The duration of the five simulation phases was $\Delta \tau_{\text{IniEq}} = \Delta \tau_{\text{Eq1}} = 500 \sigma(m/\varepsilon)^{1/2}$,
7 $\Delta \tau_{\text{In}} = 100 \sigma(m/\varepsilon)^{1/2}$, $\Delta \tau_{\text{Relax}} = 2,900 \sigma(m/\varepsilon)^{1/2}$, and $\Delta \tau_{\text{Eq2}} = 500 \sigma(m/\varepsilon)^{1/2}$. During the *In*
8 phase 50 MC insertion/removal trials were performed every 40 MD steps within the control
9 volume to prescribe the chemical potential. The vast majority of accepted MC trials were
10 insertion moves, as expected.

11
12 Each set of replicas contained 100 simulations. The initial configuration a set of replicas
13 contained 16,000 particles of component 1. Observables χ of bins at the same position n
14 and time τ of each simulation in a set of replicas were arithmetically averaged and the
15 uncertainty of each observable χ of a set of replicas was computed with the single standard
16 deviation. Observables χ sampled in each bin were averaged each $\Delta \tau = 10 \sigma(m/\varepsilon)^{1/2}$ time
17 interval. Each bin had a length in z -direction of $\Delta z_{\text{bin}} = 0.125 \sigma$ and the same quadratic
18 cross section in x - and y -direction as the simulation box. Overall, the simulation box was
19 discretized in z -direction into 1,200 bins. The rectangular measurement volumes MV_{liq} and
20 MV_{vap} had a length in z -direction of $\Delta z_{MV} = 1 \sigma$ and had a quadratic cross section with the
21 same side length as the simulation box in x - and y -direction. The two measurement volumes
22 were positioned at a distance of $\Delta z_{\text{off}} = 7 \sigma$ from the characteristic interface positions z_{10} and
23 z_{90} (cf. Eq. (1) and Figure 2), respectively. The molar fluxes in and out of the measurement
24 volumes were sampled at the boundaries of the measurement volume in positive and negative
25 z -direction. In the further course of this work for each measurement volume only the molar
26 flux at the boundary closest to the interface is shown and discussed. The simulations in this
27 work were carried out using the open source molecular dynamics code *ls1*⁸².

28 29 30 31 32 33 34 35 36 37 38 39 40 41 42 43 44 45 46 47 48 49 50 51 52 53 54 55 56 57 58 59 60

IV. RESULTS AND DISCUSSION

In this work, for each of the two studied mixtures, the same four temperatures were investigated, which yields 8 sets of replicas, each containing 100 simulations. First, in section IV A, the results for both mixtures for the temperature $T = 0.715 \varepsilon k_{\text{B}}^{-1}$ are presented and discussed in detail. An overview of the results for other temperatures are discussed in section IV B, details and the corresponding numerical data are presented in the Supporting

Information. Table I summarizes the main simulation settings and some key simulation results for all studied sets of replicas: the temperature T and the chemical potential $\mu_{2,CV}$ prescribed in the control volume as input parameters as well as the mean number of particles N_2 inserted in the *In* phase, the vapor pressure of *Eq1* and *Eq2* as well as the vapor and liquid phase density of component 2 in the *Eq2* phase.

A. Results for the Temperature $0.715 \varepsilon k_B^{-1}$

1. Response in the Liquid and the Vapor Phase

Figure 5 presents the results obtained in the replica studies carried out for $T = 0.715 \varepsilon k_B^{-1}$ with the two mixtures A and B. Besides the mean value obtained from the averaging of the replica results, also the standard deviation is depicted. Results from the sample volumes on the vapor side (MV_{vap}) and the liquid side (MV_{liq}) are shown for three observables: the density of component 2, the flux of component 2, and the pressure.

Let us first discuss the uncertainty of the results. For both mixtures and both measurement volumes, the noise of the results for the density is of the order of 10 %, cf. Figure 5, which is low considering the difficulty of the spatially and temporally resolved measurement of a small quantity. Results of a similar quality were obtained for the pressure in the measurement volume in the vapor phase. In contrast, the uncertainty of the results for the pressure in the measurement volume in the liquid phase is high, which is not astonishing regarding the extreme sensitivity of this property^{83,84}. As the flux of component 2 was not measured directly but derived from the results for the density, no standard deviation is reported. Fast changes in the pressure and the density of component 2, that occur during and shortly after the *In* phase, would not be recognizable as physically meaningful without the averaging procedure of the set of replicas.

In the initial equilibrium state *Eq1*, which is the same for both mixtures, only component 1 is present. The component 2, which is different for mixture A and mixture B, is only added in the insertion phase *In*. Shortly after the beginning of the insertion, the density of component 2 and the pressure in the measurement volume MV_{vap} increase steeply. There is a short time-delay until the first component 2 particles reach the measurement volume MV_{vap} . As a consequence, also the molar flux of component 2 j_2 in the measurement volume

1
2
3 MV_{vap} rises steeply in both simulations. All observables shown in Figure 5 peak shortly after
4 the insertion phase has ended.
5

6
7 The following relaxation to the second equilibrium state $Eq2$ is different for the mixture A
8 and the mixture B, which is partially a consequence of the differences in the equilibrium
9 state $Eq2$ for the two mixtures. The solubility of the light-boiling component 2 in the liquid
10 component 1 is significantly lower for mixture A than for mixture B^{71,73}. This is caused by
11 the lower value of ε_2 (causing a higher volatility of component 2), as well as by the lower value
12 of ξ_{12} (less favorable mixed dispersive interactions) in mixture A. As a consequence, the final
13 values of the density ρ_2 in the liquid phase are much lower for mixture A than for mixture B
14 (Figure 5 (b)), while it is vice-versa for the gas phase (Figure 5 (a)). The higher amount of
15 component 2 in the gas phase also causes the higher pressure observed for mixture A in the
16 final equilibrium state $Eq2$ (Figure 5 (e) and (f)). As expected, that pressure is the same in
17 both measurement volumes. The lower solubility of component 2 in mixture A also explains
18 why the integral under the molar flux of component 2 in the measurement volume in the
19 liquid phase MV_{liq} shown in Figure 5 (d), is much smaller than the corresponding integral for
20 mixture B. The time constant of the relaxation process is of the same order of magnitude for
21 both studied mixtures. The relaxation for mixture B is slightly slower, which is attributed
22 to the fact, that more of component 2 has to be transferred into the liquid phase, before the
23 new equilibrium state is reached. The time-dependent changes in the pressure are basically
24 a consequence of the mass transfer, as the mechanical equilibrium is established very fast.
25
26
27
28
29
30
31
32
33
34
35
36
37

38 As explained above, there is a maximum in all observables shown in Figure 5 in the vapor
39 phase measurement volume MV_{vap} that is reached shortly after the end of the insertion
40 phase In (Figure 5 (a),(c),(e)). After passing through that maximum, for the mixture B,
41 all observables simply decay to their values in the second equilibrium state $Eq2$. At about
42 $\tau = 1,200 \sigma(m/\varepsilon)^{1/2}$, a slight change of the way the decay takes places is noticeable, which
43 is best visible as a small hump in the signal for j_2 (Figure 5 (c)).
44
45
46
47
48

49 The corresponding findings for mixture A are completely unexpected: after having passed
50 the maximum, the density ρ_2 measured in MV_{vap} for mixture A first decreases and then
51 rises again to approach its value in the equilibrium state $Eq2$ (Figure 5 (a)). This oscillating
52 behavior translates into a net flux of component 2 that is first directed towards the vapor-
53 liquid interface ($j_2 > 0$), but then, for a short period in time, goes in the reverse direction
54 ($j_2 < 0$), to then turn back to the expected direction again ($j_2 > 0$) (Figure 5 (c)). The
55
56
57
58
59
60

1
2
3 negative flux of j_2 can be interpreted as a reflection of particles of component 2 at the
4 vapor-liquid interface, i.e. an important part of the particles of component 2 that are reaching
5 the interface cannot enter the liquid phase. This is related to several effects: firstly, the low
6 solubility of component 2 in the liquid phase of mixture A, that obviously hinders the uptake
7 of component 2 by the liquid phase, and, secondly, the enrichment that builds up in the
8 interfacial region in mixture A, as will be discussed below in more detail. The low affinity of
9 the liquid phase to component 2 in mixture A is a consequence of the choice of the molecular
10 parameters (low values of ε_2 and ξ_{12} for mixture A). In the discussion of the decay of the
11 signals for mixture B, we have mentioned a slight change at about $\tau = 1,200 \sigma(m/\varepsilon)^{1/2}$. This
12 could be due to a similar effect as the one observed for mixture A, which, however, is much
13 milder for mixture B, as the solubility of component 2 in the liquid phase is much better for
14 that mixture.
15
16
17
18
19
20
21
22
23
24
25
26

27 The fact that particles can be repelled from a vapor-liquid interface has been reported by
28 previously Garret et al.⁶⁶, who considered, however, equilibrium conditions, in which they
29 tracked individual particles (e.g. OH and O₃ radicals at water-air interfaces^{85,86}). To the
30 best of our knowledge, this effect has never before been observed in mass transfer studies.
31 Due to the symmetry of the overall simulation scenario, the repelled particles are once again
32 repelled at the symmetry plane in the middle of the vapor phase, which could explain the
33 small oscillations that were observed mainly in the signal for the flux j_2 in the vapor phase
34 measurement volume MV_{vap} (Figure 5 (c)).
35
36
37
38
39
40
41
42
43

44 Figure 6 shows the transient response in the pressure-composition diagram at $T =$
45 $0.715 \varepsilon k_B^{-1}$ for both studied mixtures. The pressure sampled in the liquid and vapor mea-
46 surement volume is shown as a function of composition x_2 and time τ . The liquid and vapor
47 phase state points of both *Eq1* (before the insertion) and *Eq2* (after the insertion and relax-
48 ation) have the same pressure, as expected in a vapor-liquid equilibrium. The *Eq1* and *Eq2*
49 points of the vapor and liquid domain agree well with the dew and bubble lines calculated
50 with the PeTS EOS^{10,80}. The pressure sampled in the liquid phase has high noise compared
51 to data from the vapor phase, which is typical for pressure sampled in liquid phases (cf.
52 Figure 5 (e) and (f)).
53
54
55
56
57
58
59
60

2. Response at the Vapor-Liquid Interface

Figure 7 shows spatial profiles of the density ρ_2 and the molar flux j_2 of component 2 in the vicinity of the interface and the neighboring bulk phases for both mixtures at $T = 0.715 \varepsilon k_B^{-1}$. The spatial profiles are discretized in time with an interval of $\Delta\tau = 100 \sigma(m/\varepsilon)^{1/2}$. The measured spatial profiles for each time step were superimposed at the interface position $z_{50}(\tau)$ to decrease the influence from fluctuations of that position. The *In* phase starts at $\tau = 1,000 \sigma(m/\varepsilon)^{1/2}$. The profiles measured before this time are essentially identical and represent the initial equilibrium state *Eq1*, in which no component 2 is present.

We will discuss the results for mixture B first. For that mixture, a temporary density peak of component 2 builds up in the interfacial region, cf. Figure 7 (b). Within the interfacial region, which is basically determined here by density profiles of component 1 (cf. Section II B), this peak is shifted towards the liquid side of the interface. At about $\tau = 1,400 \sigma(m/\varepsilon)^{1/2}$, this temporary density peak reaches its maximum height and then decays and finally vanishes in the equilibrium density profile of component 2 for the equilibrium state *Eq2*, that shows no extrema.

The temporary density peak of component 2 at the interface for mixture B can be interpreted as a kind of jamming. The insertion of the particles of component 2 creates an important flux j_2 in the vapor phase that is directed towards the interface. There is only little friction in the gas phase, so the particles of component 2 reach the interface with a high directed velocity. At the interface, they are slowed down by the particles in the liquid. The transport of component 2 in the liquid phase is diffusion-controlled and slower than the gas phase transport. This leads to a temporary accumulation of component 2 near the interface, which, however, vanishes as the overall transport goes to zero upon approaching the equilibrium state *Eq2*.

For mixture B, the molar flux j_2 is positive at all times and all locations as expected (the flux is always directed from the gas phase to the liquid phase). However, the flux is far from being uniform in the volume shown in Figure 7, which extends 10σ to both sides of the vapor-liquid interface. The flux j_2 measured on the vapor side shortly after the insertion are very large, but they decay quickly ($\tau < 500 \sigma(m/\varepsilon)^{1/2}$) by almost an order of magnitude of the process. The further decay to zero is then slower.

In interpreting the j_2 -flux curves, it has to be considered, that a negative slope in the

1
2
3 profile shown in Figure 7 indicates that component 2 accumulates over time in the considered
4 element, a constant profile indicates a steady state, and a positive slope indicates depletion.
5 In general, as expected, a depletion is observed on the vapor side and an accumulation on
6 the liquid side (disregarding the details related to the build-up and vanishing of the density
7 peak discussed above). The exception is the profile measured at $\tau = 1, 100 \sigma(m/\varepsilon)^{1/2}$ on the
8 vapor side where an accumulation is observed, which is due to the fact that the insertion
9 phase just stopped.

15 Also for mixture A, a peak builds up in the concentration profile of component 2 near
16 the interface shortly after the insertion phase *In* is finished. But this peak in mixture A
17 is of different nature than the one in mixture B – it does not vanish and persists also in
18 the equilibrium state *Eq2*. The peak observed in mixture A is caused by the well-known
19 enrichment of light-boiling components at vapor-liquid equilibrium interfaces¹⁻¹³, which is
20 known to be important for mixture A, but not for mixture B^{10,72}. In mixture A, the enrich-
21 ment peak builds up very quickly (in about $200 \sigma(m/\varepsilon)^{1/2}$) and then undergoes only minor
22 changes during the rest of the process (it diminishes slightly, but the difference between the
23 maximal height and the end height are only of the order of 10 %). In contrast to the peak
24 observed in mixture B, the enrichment peak in mixture A is almost symmetric with respect
25 to the interface, which confirms previous findings⁷².

35 The flux j_2 measured in mixture A shortly after the end of the insertion period *In* (at
36 $\tau = 1, 100 \sigma(m/\varepsilon)^{1/2}$) is similar to that measured in mixture B, which is not unexpected, as
37 the disturbance is then still limited largely to the vapor phase. However, for larger times,
38 major differences occur. First, the flux j_2 is much lower for mixture A than for mixture B,
39 which can be interpreted as a consequence of the lower solubility of component 2 in the
40 liquid in mixture A. Furthermore, it can be seen that at $\tau = 1, 200 \sigma(m/\varepsilon)^{1/2}$ the flux j_2 is
41 reversed in the vapor phase, i.e. there is a net flow of component 2 from the surface back
42 to the vapor. This effect has been discussed already above and is interpreted as a reflection
43 of particles of component 2 at the interface. It may be associated to the build-up of the
44 interfacial enrichment.

52 The temporary density peak of mixture B at the interface position might also be caused
53 by a higher solubility due to the increased pressure. The bubble line of mixture B has a
54 flat positive slope (cf. Figure 6 right). Hence, an increase in pressure significantly increases
55 the mole fraction of component 2 in the liquid phase of mixture B in an equilibrium state,
56
57
58
59

1
2
3 i.e. the solubility of component 2 in the liquid phase increases. The pressure in the vapor
4 phase of mixture B is higher than the pressure of the second equilibrium state $Eq2$ up to $\tau =$
5 $1,700 \sigma(m/\varepsilon)^{1/2}$, cf. Figure 5 (d), while the density peak builds up until $\tau = 1,400 \sigma(m/\varepsilon)^{1/2}$,
6 cf. Figure 7 (b). The temporarily increased pressure raises the solubility of component 2,
7 which in turn increases the molar flux across the interface and causes the temporary density
8 peak. In contrast, the slope of the bubble line of mixture A is positive and very steep
9 (cf. Figure 6 left). An increase in pressure only slightly increases the mole fraction of the
10 liquid phase of mixture A in an equilibrium state. Mixture A shows only a slight temporary
11 increased density at the interface, cf. Figure 7 (a).
12
13
14
15
16
17
18
19
20

21 B. Results for Various Temperatures

22
23

24 The new simulation method was not only used to study the mass transfer process in
25 mixture A and mixture B at the temperature $T = 0.715 \varepsilon k_B^{-1}$ but also at the temperatures
26 $T = 0.66, 0.77, 0.825 \varepsilon k_B^{-1}$. This is of particular interest since the interfacial properties of
27 the mixtures are known to depend strongly on the temperature^{10,71}, e.g. the enrichment of
28 mixture A is known to decrease with increasing temperature.
29
30
31
32

33 Figure 8 shows the results for the density of component 2 as a function of time sampled
34 in the measurement volumes in the vapor phase (MV_{vap} , top) and liquid phase (MV_{liq} ,
35 bottom) for both mixtures A and B, for all studied temperatures. In all cases, the change
36 in temperature leads to quantitative changes, but the qualitative behavior is the same for
37 all temperatures, which is not unexpected. Overall, the influence of the temperature on the
38 results is larger for mixture B, mainly as the solubility of component 2 in the liquid depends
39 on temperature for that mixture, whereas it is hardly temperature-dependent for mixture A,
40 cf. Figure 8 (c).
41
42
43
44
45
46

47 It is interesting to note that, contrary to the overall trend, the height of the initial peak
48 in the density ρ_2 measured in the vapor phase (MV_{vap}) in mixture A depends strongly on
49 temperature: the peak is large for low temperatures and almost vanishes at the highest
50 studied temperature. Together with the fact that the solubility of component 2 in the liquid
51 phase is hardly temperature-dependent, this is a strong argument for the influence of the
52 enrichment on this peak, namely as the enrichment is known to be high at low temperatures
53 and vice versa^{10,71}. This argument is further supported by the findings for mixture B for
54
55
56
57
58
59
60

1
2
3 the density ρ_2 in MV_{vap} , where the influence of the temperature on the peak height is quite
4 low, despite the considerable influence on temperature on the solubility.

5
6 Figure 8 shows the flux of component 2 sampled at different positions in the simulation
7 box as a function of time in replica simulations at various temperatures for mixture A (left)
8 and mixture B (right). Results for three positions are reported: the measurement volume on
9 the vapor side (MV_{vap}), the interfacial plane ($z = z_{50}$, see Section II B), and the measurement
10 volume on the liquid side (MV_{liq}). The results confirm that the variation of the temperature
11 leads to quantitative changes, but the qualitative behavior remains the same. Differences in
12 the flux of component 2 caused by a variation of the temperature are mainly limited to the
13 first peak in the flux observed shortly after the insertion phase. In remarkable agreement,
14 in basically all cases shown in Figure 8, the peak is highest for the lowest temperature and
15 its height decreases steadily with increasing temperature. The only exception from this rule
16 is the density signal from the liquid side MV_{liq} for mixture A, which, albeit, exhibits only a
17 very small peak.

18
19 Additional results for the temperature dependency of the transient response are given in
20 the Supporting Information.

21 22 23 24 25 26 27 28 29 30 31 32 33 34 **V. CONCLUSIONS**

35
36 A non-stationary molecular dynamics simulation method is introduced for studying mass
37 transfer through vapor-liquid interfaces. The mass transfer of a certain component through
38 the interface is driven by a concentration gradient of the respective component that is initially
39 build up and then the system relaxes in a new equilibrium state. During that relaxation
40 process, the mass transfer through the vapor-liquid interface is examined in detail. The
41 statistics of the sampling of the observables is amplified by studying sets of simulation
42 replicas, which only differ in their initial velocity distribution.

43
44 In the proposed simulation method, particles of component 2 are inserted in the middle
45 of the vapor phase of an equilibrated vapor-liquid system containing only particles of com-
46 ponent 1 over a short period of time. After the insertion phase, the system is re-equilibrated.
47 During this relaxation phase, the inserted particles move from the vapor phase through the
48 vapor-liquid interface and enter the liquid phase. Over the whole simulation run, profiles
49 of the density, composition, and mass flux of each component as well as the pressure are
50
51
52
53
54
55
56
57
58
59
60

1
2
3 sampled.
4
5
6
7

8 The simulation method was tested on binary mixtures of simple fluids. Two binary LJTS
9 mixtures with the same high-boiling component and different low-boiling components were
10 investigated. Both mixtures show distinctly different phase behaviors and interfacial prop-
11 erties such as the enrichment^{10,71}, while having a comparable bulk diffusivity²². Mixture A
12 shows a high enrichment, while mixture B shows none. The number of inserted particles
13 is chosen the same for the two studied mixtures. Even though both mixtures have similar
14 bulk phase diffusivities, the results from both mixtures from the new simulation method are
15 distinctly different, which can be attributed to differences in the interfacial properties. The
16 behavior of the mass flux across the interface deviates significantly between the two studied
17 mixtures: For mixture A, an important part of the particles are repelled at the interface.
18 The repulsion of particles at the interface causes a temporarily negative net flux back into
19 the vapor phase. No temporary negative flux is observed for mixture B. For mixture B, on
20 the other hand, a temporary density peak is observed at the beginning of the relaxation
21 process on the liquid side of the interface. This temporary accumulation of component 2
22 particles at the interface is caused by jamming due to a lower transport resistance at the
23 interface and in the liquid bulk phase compared to the vapor bulk phase. The different
24 behavior of mixture A and B is attributed to three facts: (i) the mass transfer process is
25 governed by the bulk properties of the second equilibrium state, which in turn is dependent
26 on the number of inserted particles and of course the mixture, (ii) a significant amount of
27 particles of component 2 is repelled at the interface in the case of mixture A; (iii) the en-
28 richment acts as a mass transfer resistance. Yet, the significance of the last two phenomena
29 have to be evaluated in further studies.
30
31
32
33
34
35
36
37
38
39
40
41
42
43
44
45
46
47
48

49 The results from this work strongly support the hypothesis that interfacial properties
50 influence the mass transfer through fluid interfaces. The resistance to mass transfer at the
51 interface is a dynamic property and can eventually become high enough to temporarily reduce
52 or completely stop flux through the interface and accordingly particles are repelled at the
53 interface. The non-stationary simulation method proposed in this work is a valuable tool for
54 further investigations, e.g. for studying real substance mixtures and liquid-liquid interfaces.
55
56
57
58
59
60

ACKNOWLEDGMENTS

The authors gratefully acknowledge funding of the present work by the ERC Advanced Grant ENRICO (grant agreement No. 694807). The present work was conducted under the auspices of the Boltzmann-Zuse Society of Computational Molecular Engineering (BZS) and the simulations were carried out on the Regional University Computing Center Kaiserslautern (RHRK) under the grant TUK-MTD as well as the Leibniz Supercomputing Centre (LRZ) under the grant (AMSEL)² (pn56mo).

TABLES & FIGURES

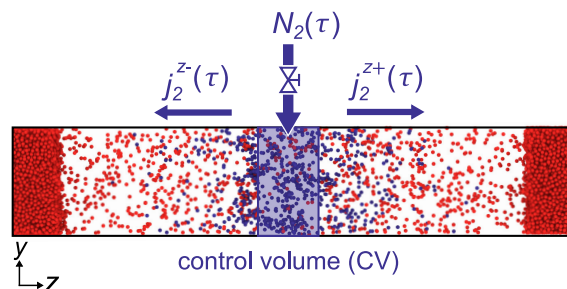


FIG. 1: Scheme of the non-stationary simulation scenario. The snapshot is taken from a simulation during the insertion phase. Prior to the insertion, the system contains only particles of the high-boiling component 1 (red). Particles of component 2 (blue) are inserted into the control volume (blue shaded area), then spread through the vapor phase, cross the vapor-liquid interface, and enter into the liquid phase until a new equilibrium state is established.

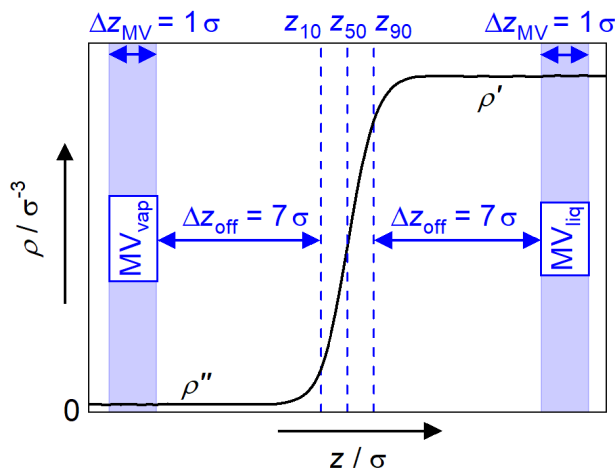


FIG. 2: Schematic of the geometric configuration of the measurement volumes (MV) located in the vicinity of the interface; showing the total density at the interface as a function of the z -direction (—). The vapor and liquid measurement volume (blue shaded areas) are located at a distance of $\Delta z_{\text{off}} = 7\sigma$ to the characteristic interface points z_{10} and z_{90} , respectively. The positions z_{10} , z_{50} and z_{90} (---) are defined according to Eq. (1).

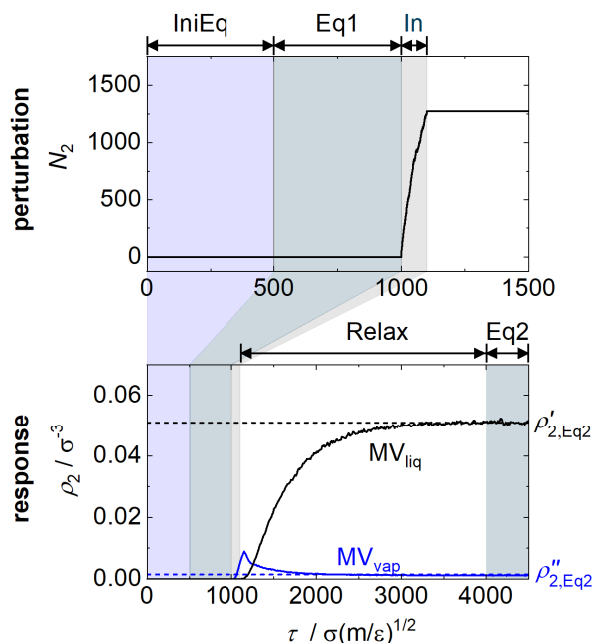


FIG. 3: Example for results from the evaluation of a set of replicas of simulation runs used here for illustrating the simulation phases. Top: number of inserted particles of component 2 N_2 as a function of the simulation time (perturbation of the system); Bottom: density of component 2 in the measurement volumes MV_{vap} and MV_{liq} (cf. Figure 2) as a function of the simulation time (response of the system). The dashed lines indicate the equilibrium states at the end of the relaxation (*Eq2*).

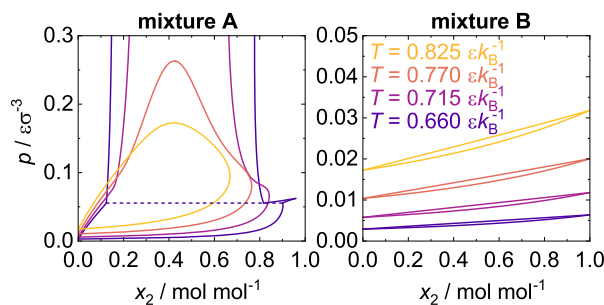


FIG. 4: Phase diagrams of mixture A (left) and mixture B (right) for all investigated temperatures calculated with the PeTS EOS^{10,80}.

TABLE I: Selected input parameters and results from the NEMD simulations for mixtures A and B carried out in the present work. Input: the temperature T in the whole simulation box and the chemical potential $\mu_{2,CV}$ in the control volume during insertion phase. Results: the number of inserted particles N_2 as well as vapor-liquid equilibrium properties for the initial and the final state: Pressure p and partial density of component 2 ρ_2 in the vapor phase ($''$) and the liquid phase ($'$). The uncertainty is reported in parentheses and refers to the last digits of the value. It was obtained from the standard deviation from the results from the simulations of the set of replicas.

Mixture	T $/ \varepsilon k_B^{-1}$	$\mu_{2,CV}$ $/ \varepsilon$	N_2	p''_{Eq1} $/ \varepsilon \sigma^{-3}$	p''_{Eq2} $/ \varepsilon \sigma^{-3}$	$\rho''_{2,Eq2}$ $/ \sigma^{-3}$	$\rho'_{2,Eq2}$ $/ \sigma^{-3}$
A	0.66	-0.55	1189(43)	0.0030(1)	0.0086(3)	0.0088(4)	0.0106(15)
	0.715	-0.675	1199(46)	0.0058(2)	0.0122(3)	0.0092(4)	0.0104(11)
	0.77	-0.8	1195(44)	0.0105(2)	0.0175(4)	0.0094(4)	0.0105(8)
	0.825	-0.9	1204(45)	0.0173(3)	0.0252(4)	0.0097(5)	0.0105(8)
B	0.66	-0.8	1194(66)	0.0030(1)	0.0032(1)	0.0007(1)	0.0538(26)
	0.715	-0.9	1212(64)	0.0059(2)	0.0063(2)	0.0011(1)	0.0519(26)
	0.77	-1.025	1189(65)	0.0105(2)	0.0111(2)	0.0018(2)	0.0485(26)
	0.825	-1.15	1184(59)	0.0173(3)	0.0183(4)	0.0026(2)	0.0455(23)

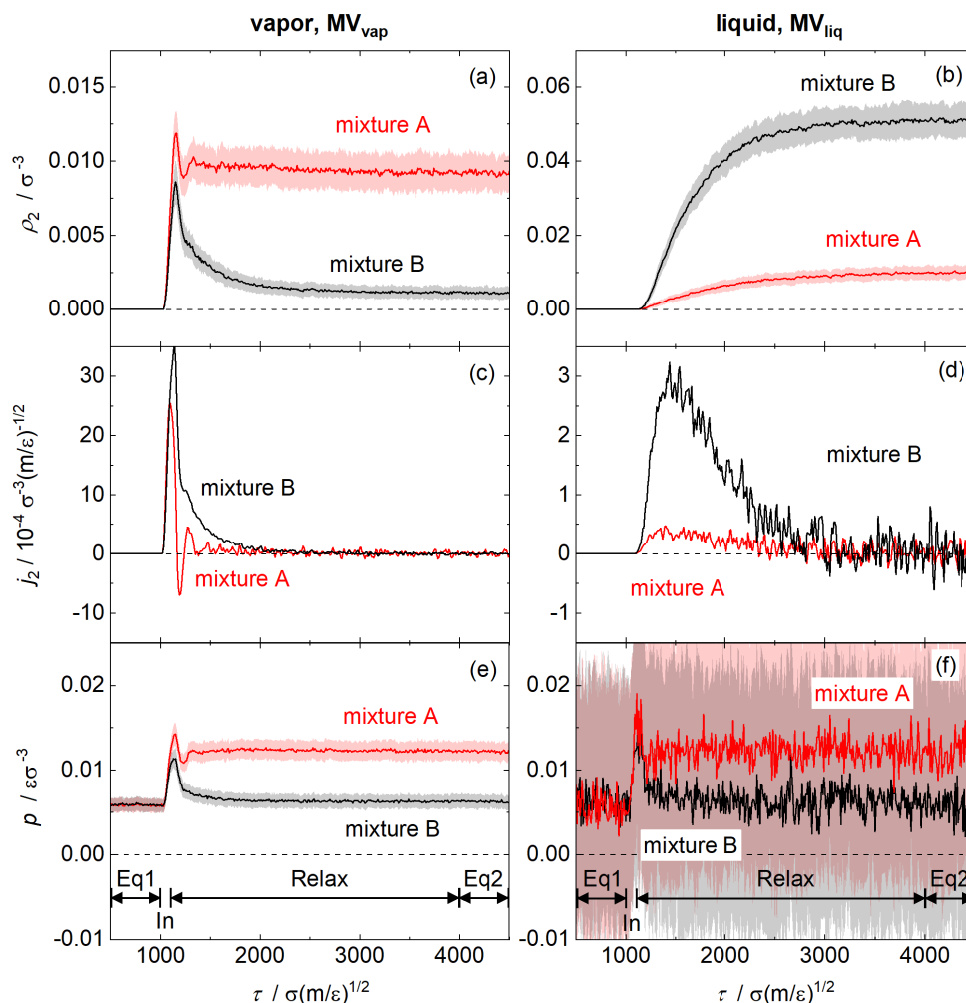


FIG. 5: Observables sampled in the replica NEMD simulations in the measurement volumes in the vapor phase MV_{vap} (left) and in the liquid phase MV_{liq} (right), respectively, as a function of the simulation time: density of component 2 ρ_2 , flux of component 2 j_2 , and pressure p . The temperature was $T = 0.715 \epsilon k_B^{-1}$. Results for mixtures A are indicated in red; results for mixtures B in black. Solid lines indicate the mean value obtained from the set of replicas, the shaded area indicates standard deviation. The standard deviation is only given for the two properties that were sampled directly (ρ_2 and p); j_2 was calculated from ρ_2 .

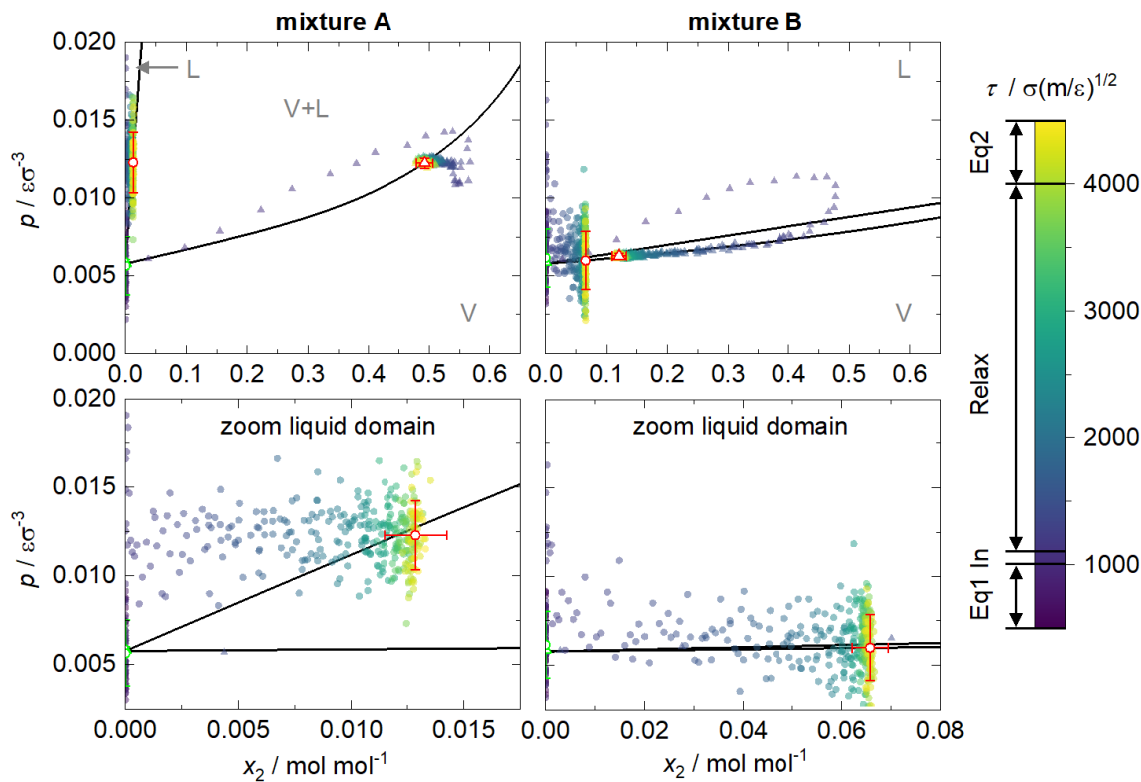


FIG. 6: Pressure-composition diagram at $T=0.715 \varepsilon k_B^{-1}$ for mixtures A (left) and mixtures B (right). Circles indicate state points sampled in the measurement volume MV_{liq} ; triangles indicate state points sampled in the measurement volume MV_{vap} . The bottom plots give a detailed view on the state points sampled in the liquid phase. The color scale indicates the simulation time. Each data point represents the mean value obtained from a set of replicas at a given simulation time τ . The white filled symbols indicate pressure and composition in *Eq1* (green) and in *Eq2* (red) phase. The error bars are the standard deviation obtained from a set of replicas. The black line indicates the phase equilibrium computed with the PeTS EOS^{10,80}.

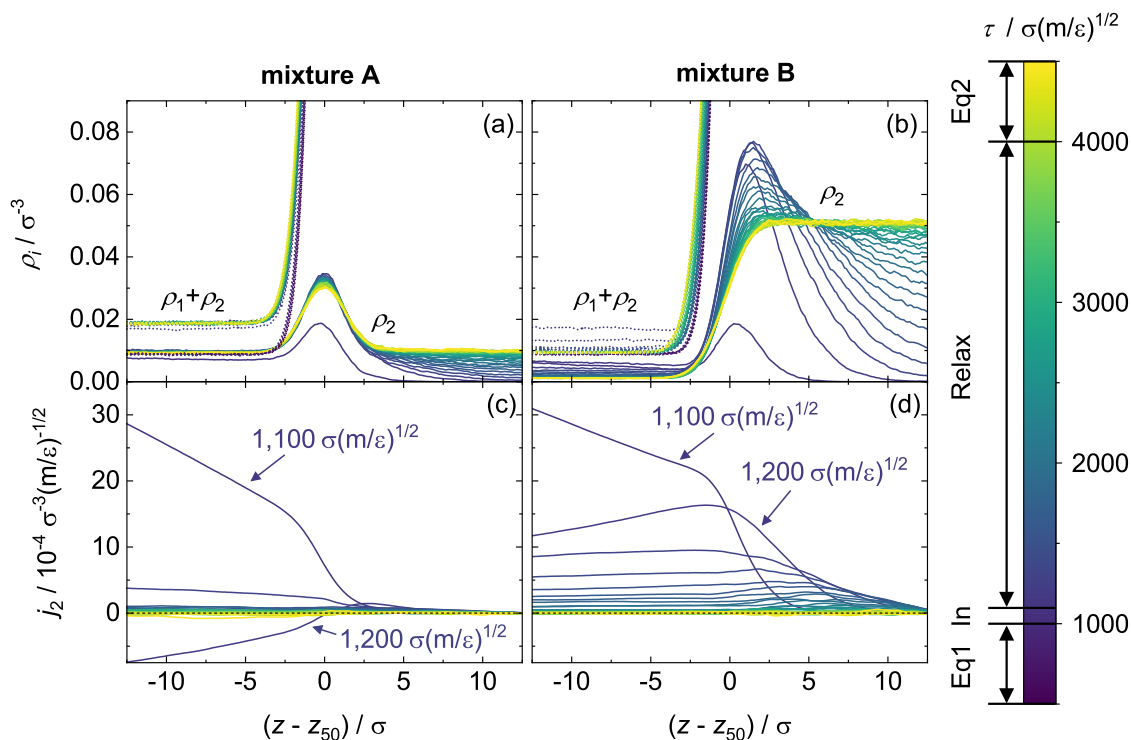


FIG. 7: Spatial profiles of the observables sampled in the vicinity of the interface and the neighboring bulk phases for mixture A (left) and mixture B (right). Results for the temperature $T = 0.715 \epsilon k_B^{-1}$ from replica simulations. Top: density of the low-boiling component 2 (—) and total density (⋯); Bottom: molar flux of component 2 j_2 . The simulation time τ is indicated by the color. The shown profiles were measured at time intervals of $\Delta\tau = 100 \sigma(m/\epsilon)^{1/2}$.

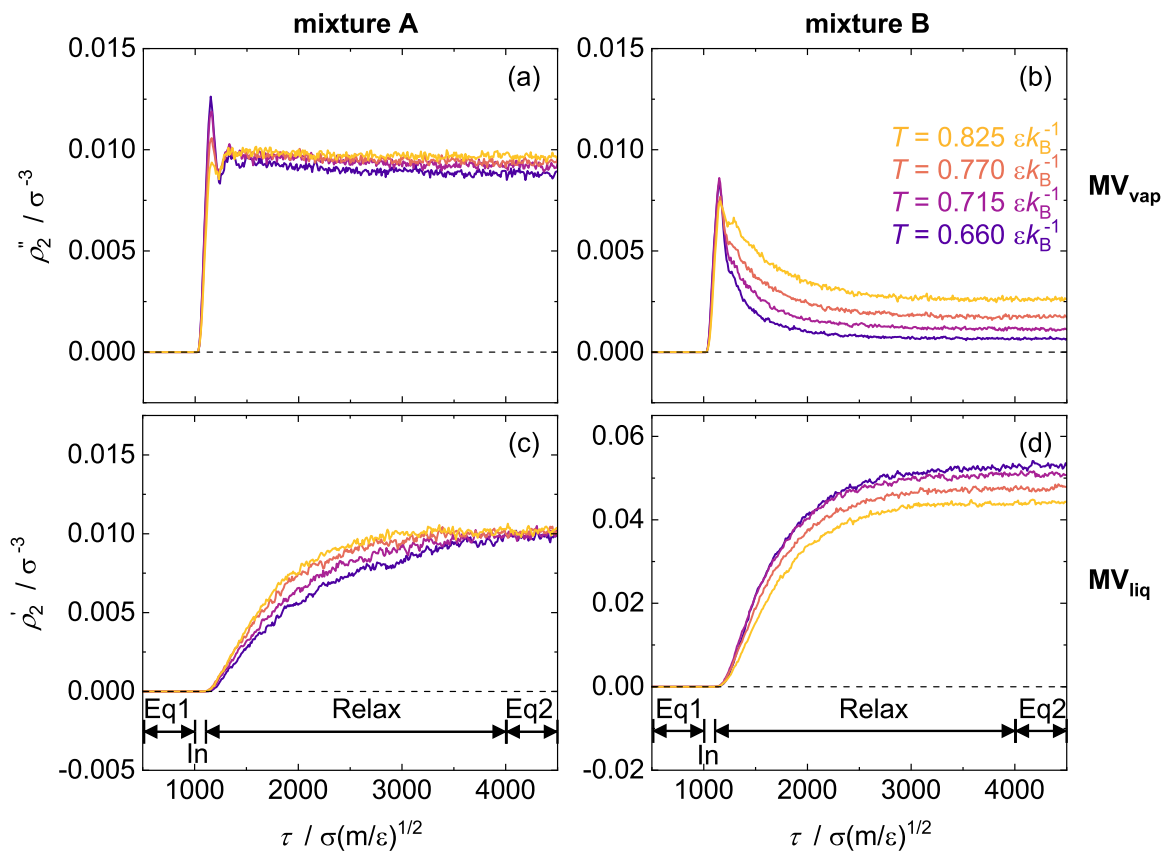


FIG. 8: Density of component 2 sampled in the measurement volume in the vapor phase MV_{vap} (top) and in the measurement volume in the liquid phase MV_{liq} (bottom) as a function of the simulation time τ . Results for mixture A (left) and mixture B (right) from replica simulations at different temperatures are shown, which are indicated by color.

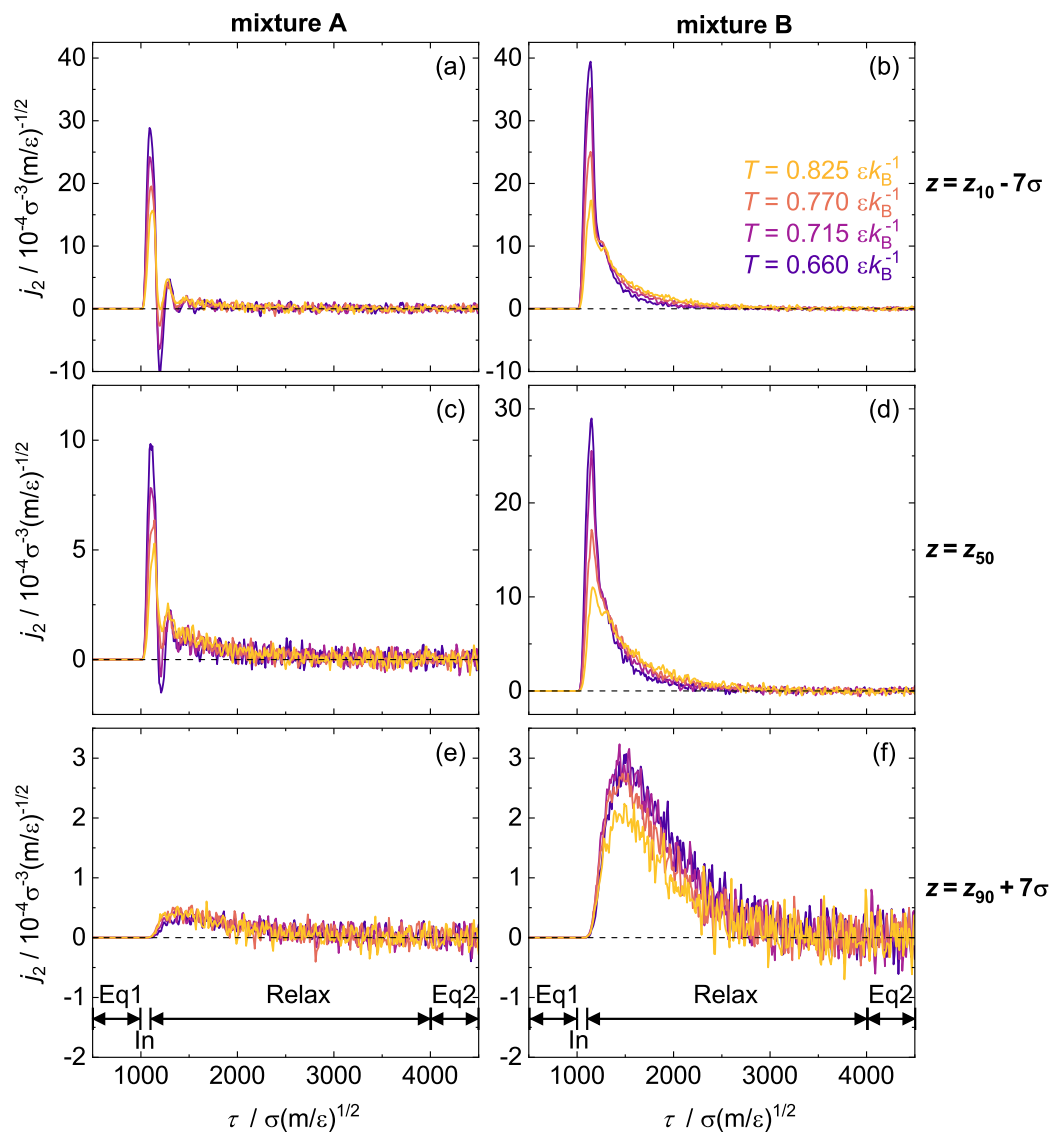


FIG. 9: Molar flux of component 2 sampled at different positions as a function of time in replica simulations at different temperatures for mixture A (left) and mixture B (right). The temperature is represented by the color. Top: measurement volume on the vapor side (MV_{vap}); Middle: interface plane $z = z_{50}$, Bottom: measurement volume on the liquid side (MV_{liq}).

REFERENCES

- ¹S. Becker, S. Werth, M. Horsch, K. Langenbach, and H. Hasse, "Interfacial tension and adsorption in the binary system ethanol and carbon dioxide: Experiments, molecular simulation and density gradient theory," *Fluid Phase Equilibria* **427**, 476 (2016).
- ²W. Li and Z. Jin, "Molecular dynamics simulation of natural gas-water interfacial tensions over wide range of pressures," *Fuel* **236**, 480–492 (2019).
- ³W. A. Fouad and L. F. Vega, "The phase and interfacial properties of azeotropic refrigerants: the prediction of azeotropes from molecular theory," *Physical Chemistry Chemical Physics* **19**, 8977–8988 (2017).
- ⁴O. G. Niño-Amézquita, D. van Putten, and S. Enders, "Phase equilibrium and interfacial properties of water+CO₂ mixtures," *Fluid Phase Equilibria* **332**, 40 (2012).
- ⁵O. G. Niño-Amézquita and S. Enders, "Phase equilibrium and interfacial properties of water+methane mixtures," *Fluid Phase Equilibria* **407**, 143–151 (2016).
- ⁶F. Llovel, N. M. Dowell, F. J. Blas, A. Galindo, and G. Jackson, "Application of the SAFT-VR density functional theory to the prediction of the interfacial properties of mixtures of relevance to reservoir engineering," *Fluid Phase Equilibria* **336**, 137–150 (2012).
- ⁷S. Enders and H. Kahl, "Interfacial properties of water + alcohol mixtures," *Fluid Phase Equilibria* **263**, 160–167 (2008).
- ⁸T.-M. Chang and L. X. Dang, "Liquid-vapor interface of methanol-water mixtures: A molecular dynamics study," *The Journal of Physical Chemistry B* **109**, 5759–5765 (2005).
- ⁹A. H. Falls, L. E. Scriven, and H. T. Davis, "Adsorption, structure, and stress in binary interfaces," *The Journal of Chemical Physics* **78**, 7300–7317 (1983).
- ¹⁰S. Stephan, K. Langenbach, and H. Hasse, "Interfacial properties of binary Lennard-Jones mixtures by molecular simulations and density gradient theory," *The Journal of Chemical Physics* **150**, 174704 (2019).
- ¹¹S. Stephan, S. Becker, K. Langenbach, and H. Hasse, "Vapor-liquid interfacial properties of the system cyclohexane+ CO₂: Experiments, molecular simulation and density gradient theory," *Fluid Phase Equilibria* **518**, 112583 (2020).
- ¹²E. A. Müller and A. Mejía, "Interfacial properties of selected binary mixtures containing n-alkanes," *Fluid Phase Equilibria* **282**, 68–81 (2009).
- ¹³C. Miqueu, J. M. Miguez, M. M. Piñeiro, T. Lafitte, and B. Mendiboure, "Simultaneous

- 1
2
3 application of the gradient theory and Monte Carlo molecular simulation for the investiga-
4 tion of methane/water interfacial properties,” *The Journal of Physical Chemistry B* **115**,
5 9618–9625 (2011).
6
7
- 8 ¹⁴S. Stephan, H. Cárdenas, A. Mejía, and E. A. Müller, “The monotonicity behavior of
9 density profiles at vapor-liquid interfaces of mixtures,” *Fluid Phase Equilibria* **564**, 113596
10 (2023).
11
12
- 13 ¹⁵R. Nagl, P. Zimmermann, and T. Zeiner, “Interfacial mass transfer in water-toluene sys-
14 tems,” *Journal of Chemical & Engineering Data* **2**, 328–336 (2020).
15
16
- 17 ¹⁶S. Stephan, K. Langenbach, and H. Hasse, “Enrichment of components at vapour-liquid
18 interfaces: A study by molecular simulation and density gradient theory,” *Chemical En-
19 gineering Transactions* **69**, 295–300 (2018).
20
21
- 22 ¹⁷C. Klink and J. Gross, “A density functional theory for vapor-liquid interfaces of mixtures
23 using the perturbed-chain polar statistical associating fluid theory equation of state,”
24 *Industrial & Engineering Chemistry Research* **53**, 6169–6178 (2014).
25
26
- 27 ¹⁸D. J. Lee, M. M. Telo da Gama, and K. E. Gubbins, “The vapour-liquid interface for
28 a Lennard-Jones model of argon-krypton mixtures,” *Molecular Physics* **53**, 1113–1130
29 (1984).
30
31
- 32 ¹⁹M. M. Telo da Gama and R. Evans, “The structure and surface tension of the liquid-vapour
33 interface near the upper critical end point of a binary mixture of Lennard-Jones fluids I.
34 the two phase region,” *Molecular Physics* **48**, 229–250 (1983).
35
36
- 37 ²⁰J. M. Garrido, M. M. Piñeiro, A. Mejía, and F. J. Blas, “Understanding the interfacial be-
38 havior in isopycnic Lennard-Jones mixtures by computer simulations,” *Physical Chemistry
39 Chemical Physics* **18**, 1114–1124 (2016).
40
41
- 42 ²¹B. Karlsson and R. Friedman, “Dilution of whisky - the molecular perspective,” *scientific
43 reports* **7**, 1–9 (2017).
44
45
- 46 ²²S. Stephan, D. Schaefer, K. Langenbach, and H. Hasse, “Mass transfer through vapour-
47 liquid interfaces: a molecular dynamics simulation study,” *Molecular Physics* **119**,
48 e1810798 (2021).
49
50
- 51 ²³M. Heinen, J. Vrabec, and J. Fischer, “Communication: Evaporation: Influence of heat
52 transport in the liquid on the interface temperature and the particle flux,” *The Journal of
53 Chemical Physics* **145**, 081101 (2016).
54
55
- 56 ²⁴A. Lotfi, J. Vrabec, and J. Fischer, “Evaporation from a free liquid surface,” *International
57
58
59
60*

- Journal of Heat and Mass Transfer **73**, 303 (2014).
- ²⁵S. Homes, M. Heinen, J. Vrabec, and J. Fischer, “Evaporation driven by conductive heat transport,” *Molecular Physics* **119**, e1836410 (2020).
- ²⁶R. S. Chatwell, M. Heinen, and J. Vrabec, “Diffusion limited evaporation of a binary liquid film,” *International Journal of Heat and Mass Transfer* **132**, 1296–1305 (2019).
- ²⁷M. Heinen and J. Vrabec, “Evaporation sampled by stationary molecular dynamics simulation,” *The Journal of Chemical Physics* **151**, 044704 (2019).
- ²⁸T. Tsuruta, H. Tanaka, and T. Masuoka, “Condensation/evaporation coefficient and velocity distributions at liquid–vapor interface,” *International Journal of Heat and Mass Transfer* **42**, 4107–4116 (1999).
- ²⁹S. Cheng, J. B. Lechman, S. J. Plimpton, and G. S. Grest, “Evaporation of Lennard-Jones fluids,” *The Journal of Chemical Physics* **134**, 224704 (2011).
- ³⁰J. M. Simon, D. Bedeaux, S. Kjelstrup, J. Xu, and E. Johannessen, “Interface film resistivities for heat and mass transfers integral relations verified by non-equilibrium molecular dynamics,” *The Journal of Physical Chemistry B* **110**, 18528–18536 (2006).
- ³¹J. Ge, D. Bedeaux, J. Simon, and S. Kjelstrup, “Integral relations, a simplified method to find interfacial resistivities for heat and mass transfer,” *Physica A: Statistical Mechanics and its Applications* **385**, 421–432 (2007).
- ³²J. Ge, S. Kjelstrup, D. Bedeaux, J. M. Simon, and B. Rousseau, “Transfer coefficients for evaporation of a system with a Lennard-Jones long-range spline potential,” *Phys. Rev. E* **75**, 061604 (2007).
- ³³M. Matsumoto, “Molecular dynamics simulation of interphase transport at liquid surfaces,” *Fluid Phase Equilibria* **125**, 195–203 (1996).
- ³⁴A. Kryukov and V. Levashov, “About evaporation–condensation coefficients on the vapor–liquid interface of high thermal conductivity matters,” *International Journal of Heat and Mass Transfer* **54**, 3042 – 3048 (2011).
- ³⁵M. Kon, K. Kobayashi, and M. Watanabe, “Kinetic boundary condition in vapor–liquid two-phase system during unsteady net evaporation/condensation,” *European Journal of Mechanics - B/Fluids* **64**, 81–92 (2017).
- ³⁶E. Bird and Z. Liang, “Transport phenomena in the Knudsen layer near an evaporating surface,” *Phys. Rev. E* **100**, 043108 (2019).
- ³⁷S. Kjelstrup and B. Hafskjold, “Nonequilibrium molecular dynamics simulations of steady-

- state heat and mass transport in distillation,” *Industrial & Engineering Chemistry Research* **35**, 4203–4213 (1996).
- ³⁸A. Røsjorde, S. Kjelstrup, D. Bedeaux, and B. Hafskjold, “Nonequilibrium Molecular Dynamics Simulations of Steady-State Heat and Mass Transport in Condensation. II. Transfer Coefficients,” *Journal of Colloid and Interface Science* **240**, 355–364 (2001).
- ³⁹A. Røsjorde, D. Fossmo, D. Bedeaux, S. Kjelstrup, and B. Hafskjold, “Nonequilibrium molecular dynamics simulations of steady-state heat and mass transport in condensation: I. local equilibrium,” *Journal of Colloid and Interface Science* **232**, 178–185 (2000).
- ⁴⁰I. Inzoli, S. Kjelstrup, D. Bedeaux, and J. Simon, “Transfer coefficients for the liquid–vapor interface of a two-component mixture,” *Chemical Engineering Science* **66**, 4533–4548 (2011).
- ⁴¹B. Hafskjold and T. Ikeshoji, “Non equilibrium molecular dynamics simulation of coupled heat- and mass transport across a liquid/vapor interface,” *Molecular Simulation* **16**, 139–150 (1996).
- ⁴²L. van der Ham, R. Bock, and S. Kjelstrup, “Modelling the coupled transfer of mass and thermal energy in the vapour–liquid region of a nitrogen–oxygen mixture,” *Chemical Engineering Science* **65**, 2236–2248 (2010).
- ⁴³E. Johannessen, J. Gross, and D. Bedeaux, “Nonequilibrium thermodynamics of interfaces using classical density functional theory,” *The Journal of Chemical Physics* **129**, 184703 (2008).
- ⁴⁴E. Johannessen and D. Bedeaux, “Integral relations for the heat and mass transfer resistivities of the liquid–vapor interface,” *Physica A: Statistical Mechanics and its Applications* **370**, 258–274 (2006).
- ⁴⁵K. Glavatskiy and D. Bedeaux, “Transport of heat and mass in a two-phase mixture: From a continuous to a discontinuous description,” *The Journal of Chemical Physics* **133**, 144709 (2010).
- ⁴⁶C. Klink, C. Waibel, and J. Gross, “Analysis of interfacial transport resistivities of pure components and mixtures based on density functional theory,” *Industrial & Engineering Chemistry Research* **54**, 11483–11492 (2015).
- ⁴⁷M. Lísal, J. K. Brennan, W. R. Smith, and F. R. Siperstein, “Dual control cell reaction ensemble molecular dynamics: A method for simulations of reactions and adsorption in porous materials,” *The Journal of Chemical Physics* **121**, 4901–4912 (2004).

- 1
2
3
4
5
6
7
8
9
10
11
12
13
14
15
16
17
18
19
20
21
22
23
24
25
26
27
28
29
30
31
32
33
34
35
36
37
38
39
40
41
42
43
44
45
46
47
48
49
50
51
52
53
54
55
56
57
58
59
60
- ⁴⁸G. Arya, H.-C. Chang, and E. J. Maginn, “A critical comparison of equilibrium, non-equilibrium and boundary-driven molecular dynamics techniques for studying transport in microporous materials,” *The Journal of Chemical Physics* **115**, 8112–8124 (2001).
- ⁴⁹Z. Ható, D. Boda, and T. Kristóf, “Simulation of steady-state diffusion: Driving force ensured by dual control volumes or local equilibrium monte carlo,” *The Journal of Chemical Physics* **137**, 054109 (2012).
- ⁵⁰M. G. Martin, A. P. Thompson, and T. M. Nenoff, “Effect of pressure, membrane thickness, and placement of control volumes on the flux of methane through thin silicalite membranes: A dual control volume grand canonical molecular dynamics study,” *The Journal of Chemical Physics* **114**, 7174–7181 (2001).
- ⁵¹P. Pohl, G. S. Heffelfinger, and D. M. Smith, “Molecular dynamics computer simulation of gas permeation in thin silicalite membranes,” *Molecular Physics* **89**, 1725–1731 (1996).
- ⁵²P. I. Pohl and G. S. Heffelfinger, “Massively parallel molecular dynamics simulation of gas permeation across porous silica membranes,” *Journal of Membrane Science* **155**, 1–7 (1999).
- ⁵³J. M. D. MacElroy, “Nonequilibrium molecular dynamics simulation of diffusion and flow in thin microporous membranes,” *The Journal of Chemical Physics* **101**, 5274–5280 (1994).
- ⁵⁴A. P. Thompson, D. M. Ford, and G. S. Heffelfinger, “Direct molecular simulation of gradient-driven diffusion,” *The Journal of Chemical Physics* **109**, 6406–6414 (1998).
- ⁵⁵A. P. Thompson and G. S. Heffelfinger, “Direct molecular simulation of gradient-driven diffusion of large molecules using constant pressure,” *The Journal of Chemical Physics* **110**, 10693–10705 (1999).
- ⁵⁶J. Sun and L. T. Zhang, “Temperature control algorithms in dual control volume grand canonical molecular dynamics simulations of hydrogen diffusion in palladium,” *The Journal of Chemical Physics* **127**, 164721 (2007).
- ⁵⁷G. S. Heffelfinger and F. van Swol, “Diffusion in Lennard-Jones fluids using dual control volume grand canonical molecular dynamics simulation (DCV-GCMD),” *The Journal of Chemical Physics* **100**, 7548–7552 (1994).
- ⁵⁸G. S. Heffelfinger and D. M. Ford, “Massively parallel dual control volume grand canonical molecular dynamics with LADERA I. gradient driven diffusion in Lennard-Jones fluids,” *Molecular Physics* **94**, 659–671 (1998).
- ⁵⁹G. Heffelfinger and D. Ford, “Massively parallel dual control volume grand canonical molec-

- ular dynamics with LADERA II. gradient driven diffusion through polymers,” *Molecular Physics* **94**, 673–683 (1998).
- ⁶⁰P. M. Rauscher, H. C. Öttinger, and J. J. de Pablo, “Nonequilibrium statistical thermodynamics of multicomponent interfaces,” *Proceedings of the National Academy of Sciences* **119**, e2121405119 (2022).
- ⁶¹V. G. Baidakov, S. P. Protsenko, and V. M. Bryukhanov, “Relaxation processes at liquid-gas interfaces in one- and two-component Lennard-Jones systems: Molecular dynamics simulation,” *Fluid Phase Equilibria* **481**, 1 – 14 (2019).
- ⁶²V. G. Baidakov and S. P. Protsenko, “Molecular-dynamics simulation of relaxation processes at liquid–gas interfaces in single- and two-component Lennard-Jones systems,” *Colloid Journal* **81**, 491–500 (2019).
- ⁶³K. Bucior, L. Yelash, and K. Binder, “Molecular-dynamics simulation of evaporation processes of fluid bridges confined in slitlike pores,” *Physical Review E* **79**, 031604 (2009).
- ⁶⁴C. Braga, A. Galindo, and E. A. Müller, “Nonequilibrium molecular dynamics simulation of diffusion at the liquid-liquid interface,” *The Journal of Chemical Physics* **141**, 154101 (2014).
- ⁶⁵C. Braga, J. Muscatello, G. Lau, E. A. Müller, and G. Jackson, “Nonequilibrium study of the intrinsic free-energy profile across a liquid-vapour interface,” *The Journal of Chemical Physics* **144**, 044703 (2016).
- ⁶⁶B. C. Garrett, G. K. Schenter, and A. Morita, “Molecular simulations of the transport of molecules across the liquid/vapor interface of water,” *Chemical Reviews* **106**, 1355–1374 (2006).
- ⁶⁷L. Casalino, Z. Gaieb, J. A. Goldsmith, C. K. Hjorth, A. C. Dommer, A. M. Harbison, C. A. Fogarty, E. P. Barros, B. C. Taylor, J. S. McLellan, *et al.*, “Beyond shielding: the roles of glycans in the SARS-CoV-2 spike protein,” *ACS Central Science* **6**, 1722–1734 (2020).
- ⁶⁸S. Stephan, M. Dyga, H. M. Urbassek, and H. Hasse, “The influence of lubrication and the solid–fluid interaction on thermodynamic properties in a nanoscopic scratching process,” *Langmuir* **35**, 16948–16960 (2019).
- ⁶⁹S. Stephan, M. Dyga, I. A. Alhafez, J. Lenhard, H. M. Urbassek, and H. Hasse, “Reproducibility of atomistic friction computer experiments: a molecular dynamics simulation study,” *Molecular Simulation* **47**, 1509–1521 (2021).

- 1
2
3 ⁷⁰Y. Zhang, A. Otani, and E. J. Maginn, “Reliable viscosity calculation from equilibrium
4 molecular dynamics simulations: A time decomposition method,” *Journal of Chemical*
5 *Theory and Computation* **11**, 3537–3546 (2015).
6
7
8 ⁷¹S. Stephan and H. Hasse, “Molecular interactions at vapor-liquid interfaces: Binary mix-
9 tures of simple fluids,” *Physical Review E* **101**, 012802 (2020).
10
11 ⁷²S. Stephan and H. Hasse, “Interfacial properties of binary mixtures of simple fluids and
12 their relation to the phase diagram,” *Physical Chemistry Chemical Physics* **22**, 12544–
13 12564 (2020).
14
15
16 ⁷³S. Stephan and H. Hasse, “Influence of dispersive long range interactions on properties
17 of vapour-liquid interfaces of binary Lennard-Jones mixtures,” *Molecular Physics* **118**,
18 e1699185 (2020).
19
20
21 ⁷⁴S. Stephan and H. Hasse, “Enrichment at vapour-liquid interfaces of mixtures: Establishing
22 a link between nanoscopic and macroscopic properties,” *International Reviews in Physical*
23 *Chemistry* **39**, 319–349 (2020).
24
25
26 ⁷⁵G. Rutkai, M. Thol, R. Span, and J. Vrabec, “How well does the Lennard-Jones potential
27 represent the thermodynamic properties of noble gases?” *Molecular Physics* **115**, 1104–
28 1121 (2017).
29
30
31 ⁷⁶S. Stephan, M. Horsch, J. Vrabec, and H. Hasse, “MolMod - an open access database of
32 force fields for molecular simulations of fluids,” *Molecular Simulation* **45**, 806–814 (2019).
33
34
35 ⁷⁷M. P. Allen and D. J. Tildesley, *Computer Simulation of Liquids* (Oxford University Press,
36 Oxford, 1989).
37
38
39 ⁷⁸H. A. Lorentz, “Ueber die Anwendung des Satzes vom Virial in der kinetischen Theorie
40 der Gase,” *Annalen Der Physik* **248**, 127–136 (1881).
41
42
43 ⁷⁹D. Berthelot, “Sur le mélange des gaz,” *Comptes rendus hebdomadaires des séances de*
44 *l’Académie des Sciences* **126**, 1703–1706 (1898).
45
46
47 ⁸⁰M. Heier, S. Stephan, J. Liu, W. G. Chapman, H. Hasse, and K. Langenbach, “Equation of
48 state for the Lennard-Jones truncated and shifted fluid with a cut-off radius of 2.5σ based
49 on perturbation theory and its applications to interfacial thermodynamics,” *Molecular*
50 *Physics* **116**, 2083–2094 (2018).
51
52
53 ⁸¹S. Stephan, M. Thol, J. Vrabec, and H. Hasse, “Thermophysical properties of the Lennard-
54 Jones fluid: Database and data assessment,” *Journal of Chemical Information and Mod-*
55 *eling* **59**, 4248–4265 (2019).
56
57
58
59
60

- 1
2
3
4
5
6
7
8
9
10
11
12
13
14
15
16
17
18
19
20
21
22
23
24
25
26
27
28
29
30
31
32
33
34
35
36
37
38
39
40
41
42
43
44
45
46
47
48
49
50
51
52
53
54
55
56
57
58
59
60
- ⁸²C. Niethammer, S. Becker, M. Bernreuther, M. Buchholz, W. Eckhardt, A. Heinecke, S. Werth, H.-J. Bungartz, C. W. Glass, H. Hasse, J. Vrabec, and M. Horsch, “ls1 mardyn: The massively parallel molecular dynamics code for large systems,” *Journal of Chemical Theory Computation* **10**, 4455–4464 (2014).
- ⁸³S. Werth, M. Kohns, K. Langenbach, M. Heilig, M. Horsch, and H. Hasse, “Interfacial and bulk properties of vapor-liquid equilibria in the system toluene + hydrogen chloride + carbon dioxide by molecular simulation and density gradient theory + PC-SAFT,” *Fluid Phase Equilibria* **427**, 219–230 (2016).
- ⁸⁴S. Stephan, J. Liu, K. Langenbach, W. G. Chapman, and H. Hasse, “Vapor-liquid interface of the Lennard-Jones truncated and shifted fluid: Comparison of molecular simulation, density gradient theory, and density functional theory,” *The Journal of Physical Chemistry C* **122**, 24705–24715 (2018).
- ⁸⁵M. Roeselová, J. Viecei, L. X. Dang, B. C. Garrett, and D. J. Tobias, “Hydroxyl radical at the air-water interface,” *Journal of the American Chemical Society* **126**, 16308–16309 (2004).
- ⁸⁶J. Viecei, M. Roeselova, N. Potter, L. X. Dang, B. C. Garrett, and D. J. Tobias, “Molecular dynamics simulations of atmospheric oxidants at the air-water interface: solvation and accommodation of OH and O₃,” *The Journal of Physical Chemistry B* **109**, 15876–15892 (2005).

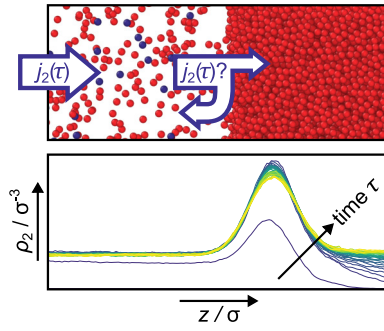


FIG. 10: For Table of Contents Only.